

# The challenge of measuring busbarless solar cells and the impact on cell-to-module losses

Michael Rauer, Alexander Krieg, Andrea Pfreundt, Max Mittag & Sebastian Pingel, Fraunhofer Institute for Solar Energy Systems ISE, Freiburg, Germany

## Abstract

The realistic measurement of solar cells is key for the whole PV industry, as accurate information about cell power is one of the most important aspects in solar cell purchase and PV module design. The omission of busbars introduces new challenges to the current–voltage measurement of solar cells, since contact to every single grid finger has to be established with independent current and voltage contacts. It is not just the shadow correction of the measurement unit that needs to be carried out more laboriously, but also the contacting of the front metal grid, which is more critical because of the high resistivity of the grid fingers. The position of the voltage sensing contact and the number of current contacts can thus have a noticeable impact on the measured performance of busbarless solar cells. Measured efficiencies are highly dependent on the contacting schemes used in different measurement systems, as these vary in contact number and sensing configuration. Two different main approaches for measuring busbarless solar cells have evolved, representing either realistic or idealized application of the cells in the module. The pros and cons of both approaches are discussed in detail in this paper. *Realistic* measurement conditions lead to efficiencies which best predict module performance, but are hard to realize and require knowledge about the subsequent module design. Although not their primary purpose, the use of *idealized* measurement conditions can make it easier to achieve record cell efficiencies, but with the disadvantage of limited comparability with busbar-based solar cell concepts. Idealized conditions can moreover lead to hidden losses in performance of the solar cells, related to the application in a module, which in turn causes inflated cell-to-module (CTM) losses. If solar cells are bought in terms of \$/Wp and modules are sold likewise, the economic implications arising from the different measurement configurations have to be considered. Whichever approach is used for the measurement of busbarless solar cells, full disclosure of the measurement configuration is absolutely essential.



Figure 1. Industrial busbarless silicon solar cell.

## Introduction

In the last few years, there has been huge progress in screen-printing technologies with regard to reducing finger widths [1]. To keep the series resistance losses resulting from increased finger resistivity low, the number of busbars has continuously increased and their width decreased, with multi-busbar concepts becoming mainstream [2]. The next step in this evolution is to omit busbars entirely (Fig. 1). Interconnection between metal grids is no longer realized by means of interconnectors soldered to busbars, as has been done until recently, but is outsourced to the module level. Tabs or wires are either soldered or glued directly to the fingers [3,4], or wires embedded in adhesive foils are soldered to the solar cells [5]. The cost savings realized through reducing the amount of silver per cell is also driving this evolution. Although the market share of busbarless solar cells is still limited, it is predicted to increase to over 30% in the next ten years [2].

The evolution to busbarless solar cells is accompanied by new challenges in manufacturing as well as in quality testing. The most important test by far is the measurement of the current–voltage ( $I$ – $V$ ) characteristics, which is a key driver for the determination of solar cell selling price, and is used for sorting the solar cells into different bins according to current or power for the subsequent module interconnection. For this measurement, temporary contacts for current extraction and voltage measurement have to be applied to the solar cells.

For conventional solar cells, well-established contacting methods are available and specified in international standards [6]. Contacting is thereby oriented towards the idealized integration of the solar cells into a module: it requires that a constant potential over the entire busbars is realized, which corresponds to an infinitely conductive interconnector. In practice, this is realized by applying a sufficient number of current contacts [7] or by smart voltage sensing at the average voltage of the potential distribution [8,9]. Moreover, the shadow caused by the contact units needs to be eliminated, which is mainly for reasons of reproducibility. Sun simulators used throughout the PV community exhibit different light divergence. The contact units therefore cast different shadows on different simulators. Without shadow correction,

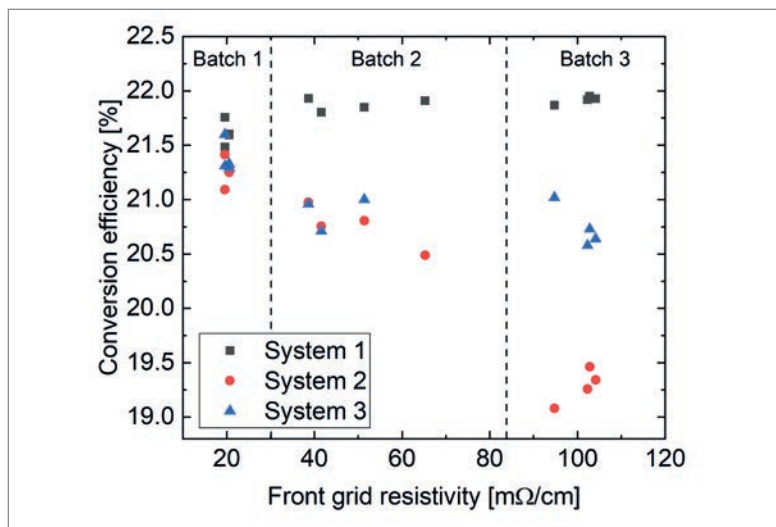


**Figure 2.** Measured conversion efficiency  $\eta$  for industrial silicon heterojunction (SHJ) solar cells with different front-grid resistivity ranges. Three different commercially available systems were used for the measurements.

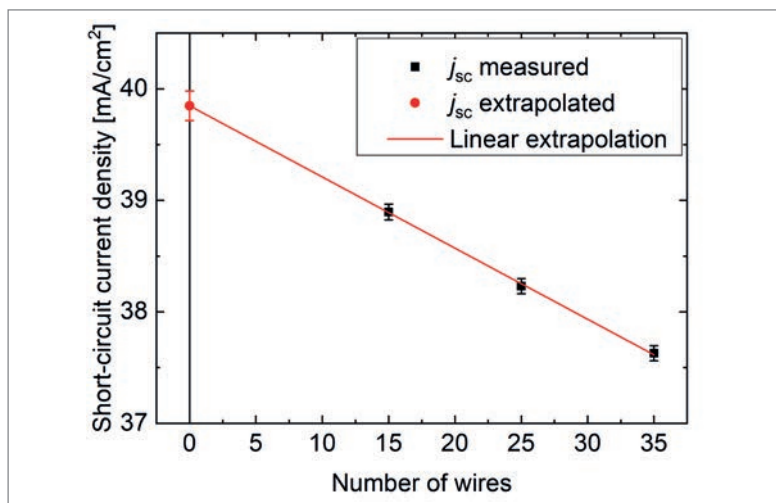


**Figure 3.** Short-circuit current density  $j_{sc}$  of a busbarless cell measured with different numbers of contact wires. The shadow-free  $j_{sc}$  can be determined by linear extrapolation to zero wires.

this could lead to false calibration of solar simulators and erroneous sorting of solar cells, if the calibration laboratory simulator and the production line  $I$ - $V$  tester exhibit different divergences. The established way of measuring cells therefore corresponds to an ideal interconnector without any shadow. The losses occurring from realistic interconnection ribbons that cast a specific shadow contribute to the so-called *cell-to-module (CTM) ratio* [10,11]. Since the shadowing losses of interconnectors are considered in CTM analyses, cell measurements require either the shadow correction in order to avoid a double consideration of interconnector shading, or a cell measurement that exactly replicates the interconnectors as used in module integration, which is unrealistic because of the wide variety of module designs.

For busbarless solar cells, things are considerably less clear and less established. Although several different measurement systems are available on the

market [12–16] or have been presented by research institutes [17,18], no common procedure for the measurement of busbarless solar cells has evolved so far. The contacting schemes realized in the systems can be very different. For some systems, only current contacts are applied to the solar cells, and the voltage is measured on the current contact bars. For other systems, both current and voltage contacts are realized on the metal grid of the solar cells, but the positioning of these contacts relative to each other can be very different from system to system. Furthermore, the systems also vary in the number of current contacts to the solar cells. All these aspects strongly affect the  $I$ - $V$  measurement results, and the effect intensifies with increasing resistivity of the metal grid [19]. Fill factor ( $FF$ ) values in particular – and thus efficiency values  $\eta$  – can vary considerably and depend on the system used for the measurement.

As there are so many different ways to perform  $I$ - $V$  measurements, this unavoidably leads to the question as to which particular value of efficiency of busbarless solar cells can be considered the most meaningful. This paper therefore discusses deviations in  $I$ - $V$  parameters by applying different contacting schemes, and gives background information on shadow correction and contacting of busbarless solar cells. The comparability with conventional, busbar-based solar cell concepts is also analysed. The implications of different measurement approaches for CTM losses are then addressed. Finally, the question of what might be the most relevant efficiency of busbarless solar cells is discussed and recommendations are given.

### Measurement systems for busbarless solar cells

To investigate the influence of the contacting scheme on the performance of busbarless solar cells, the  $I$ - $V$  characteristics of industrial bifacial busbarless silicon heterojunction (SHJ) solar cells were measured using three different industrial, commercially available systems. To further evaluate the effect of the resistivity of the front grid, solar cells with three different grid resistivity ranges were used. The measured conversion efficiencies of the SHJ cells are shown in Fig. 2. Note that the solar cells of the different resistivity groups originate from different production batches, which are based on very similar fabrication processes but vary slightly in rear-grid resistivity. The different groups can therefore not be directly compared with each other. A comparison of the measurement systems within a given group is, however, very conclusive.

Clearly, the difference in measured efficiency within a given group highly depends on the measurement system used. For low grid resistivity, the difference in  $\eta$  between the systems is relatively small; however, the higher the grid resistivity, the larger the difference becomes.

This brief experiment shows that the choice of measurement system can significantly affect the measured performance of busbarless solar cells. In the

**“No common procedure for the measurement of busbarless solar cells has so far evolved.”**

following section, the background to this effect is discussed in detail.

### Complexity of measuring busbarless solar cells

This section will provide insight into the complexity of measuring busbarless solar cells. It will deal with how measurement results need to be assessed, particularly in comparison to conventional, busbar-based solar cells.

#### Shadow correction of the measurement unit

For conventional solar cells with busbars measured at calibration laboratories, correction of the shadow by the contact unit is generally done by means of measurements with Kelvin probes [7,9,20]. These probes contact the busbars only at the rim and cast negligible shadow. This way, the shadow-free short-circuit current density  $j_{sc}$  of the solar cells can be easily measured.

For busbarless solar cells, however, the above well-established procedure cannot be used, because there are no busbars for contacting with the Kelvin probes. Instead, the shadow-free  $j_{sc}$  needs to be determined by varying the number of contact bars or wires, which is more laborious. Fig. 3 shows the  $j_{sc}$  values measured using a wire-based contact unit and different numbers of wires. Since each wire casts a certain amount of shadow onto the solar cell, the measured  $j_{sc}$  decreases when the number of wires increases. By linear extrapolation to zero wires, the shadow-free  $j_{sc}$  can then be determined.

For monocrystalline solar cells with pseudo-square rounding of the edges, the area covered by the wires may be a more precise measure for the shadow than merely the number of contacts.

#### Influence of the voltage sensing position

Contacting busbarless solar cells is, from a metrology point of view, much more complex than contacting conventional solar cells with busbars. For busbarless solar cells, the contacting unit not only needs to ensure contact to every single grid finger, but also needs to provide independent current and voltage contacts, which are ideally located directly on the metal grid.

The positioning of the current and voltage contacts significantly affects the measured  $I-V$  characteristics [8,19]. Fig.4(a) shows a schematic of the contacting situation: the finger collects the current from the photoactive area and conducts it to the current contact. The cumulative current in the finger thus increases towards the current contact and is highest directly at the contact. As the finger exhibits a distinct resistivity, the current flow leads to a voltage drop along the finger. Fig. 4(b) shows voltage distributions in the finger, which have been iteratively calculated using a model of independent diodes interconnected by resistors [19] for the industrial SHJ solar cells measured in the previous section. Different voltage sensing positions were considered for the calculations, as well as a grid resistivity of  $50\text{m}\Omega/\text{cm}$  (finger resistivity of  $4.0\Omega/\text{cm}$ ) and nine current contact wires or bars over the



## SOLAR PV MODULES MANUFACTURING LINES



Turnkey solutions from 80MW to 1GW

Solutions and services throughout the entire value chain:

- Tabber & Stringer
- Interconnection
- Laminator
- PV Module Testing
- General automation
- Customized solutions
- Full service package
- Training and know-how transfer
- High production capacity

Suitable for different technologies and cell types:

- Double glass, Cut-cells, and BIPV
- PERC, PERT, HJT, TOPCon and Bifacial cell types
- Cell size: Up to M12

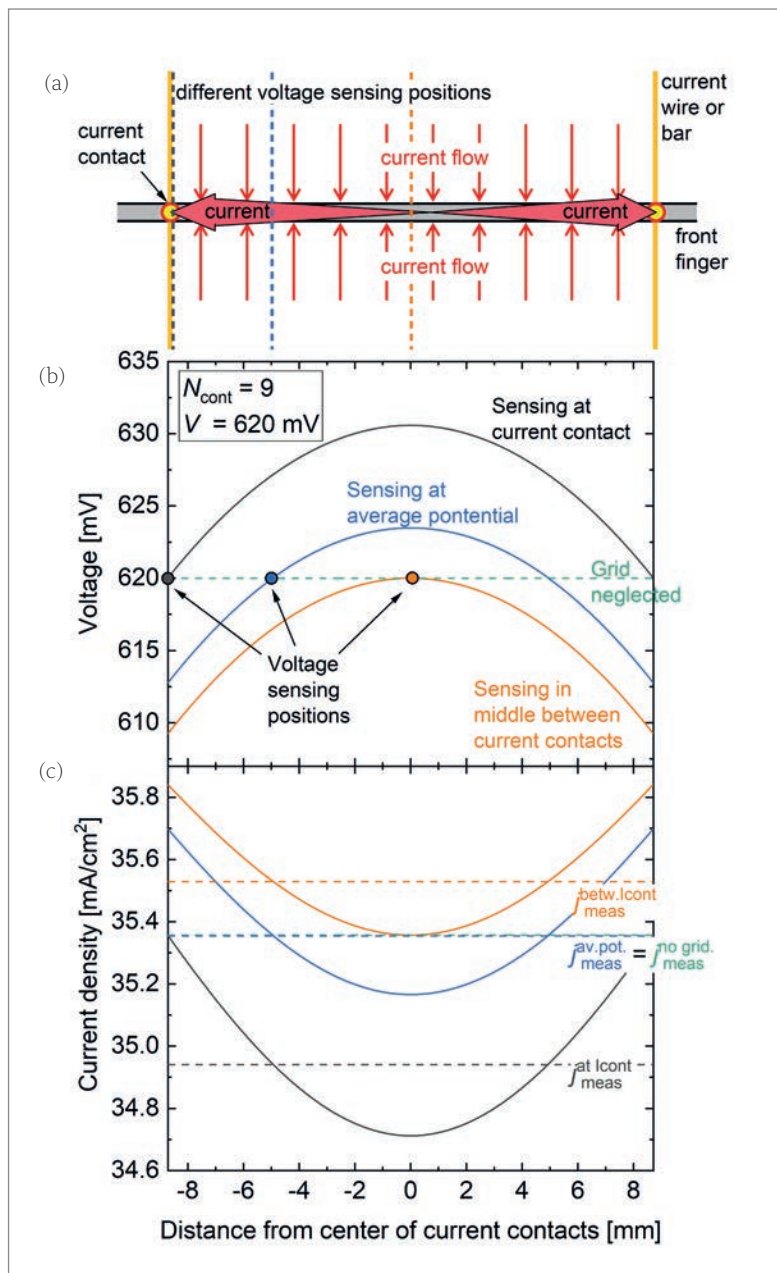


**Figure 4. (a) Schematic contacting of a grid finger with current wires or bars. A perpendicular current flow into the finger is assumed, which leads to an increase in cumulative current towards the current contact. The dashed lines represent three different voltage sensing positions. (b) Calculated voltage distributions in the contact finger (finger resistivity of  $4\Omega/\text{cm}$ , grid resistivity of  $50\text{m}\Omega/\text{cm}$ ) for the three different voltage sensing positions. The measured voltage is the same for all configurations and is close to the maximum power point. (c) Calculated current density distribution for the different sensing configurations. The current density measured at the current contact is the average over the distribution and is indicated by the dashed lines.**

solar cell. For simplicity, the solar cells were assumed to be monofacial with a fully metalized rear. For the distributions shown in Fig. 4(b), it is assumed that the voltage source is set to the same voltage, so that a voltage of  $620\text{mV}$  is measured at the voltage contact for all sensing configurations, i.e. one distinct voltage point on the  $I$ - $V$  curves was regarded. This voltage is close to the maximum power point (mpp).

**“Contacting busbarless solar cells is, from a metrology point of view, much more complex than contacting conventional solar cells with busbars.”**

The voltage distributions in the fingers generally exhibit a parabolic form, which results from the product of a – by first approximation – linear increase in cumulative current in the finger and a linear increase in finger resistance. The dashed green line additionally shows the distribution for the case when the resistance of the front grid is set to zero; this is referred to as the *grid-neglected* case, which leads to a flat distribution with homogeneous potential in the finger.

Although the voltages measured at the external voltage contact are identical for all sensing configurations, it is evident that the voltage distributions in the finger are very different. This also affects the current density distributions in the fingers, which are shown in Fig. 4(c). The current density measured at the external current contact is not the one occurring locally at the current contact, but the average over the entire distribution in the finger [8,19]. The dashed lines in Fig. 4(c) show that the measured current densities differ significantly for the different voltage sensing positions. This means that, although the measured voltages are the same, the measured current densities are highly dependent on the voltage sensing scheme.

For sensing at the current contact, the measured current density is lower than that measured for the grid-neglected case. This holds true not only for  $V = 620\text{mV}$  but for all voltage points of the mpp region, which is shown in Fig. 5. The voltage points of the  $I$ - $V$  curves around the short-circuit and open-circuit points are not affected, as there is no slope of the  $I$ - $V$  curve and no current flowing, respectively. The effect of reduced current densities in the mpp region is known as a *distributed series resistance* of the finger grid [21,22] and reduces the measured  $FF$ . For sensing in the middle, between two current contacts, the current density in the mpp region is higher than that for the grid-neglected case; correspondingly, the measured  $FF$  is higher as well.

As Fig. 4 shows, there is one specific voltage sensing position, which is at approximately 22% of the distance between two current contacts [8], for which the measured current density equals the current density of a grid-neglected measurement. Setting the voltage contact to this position therefore corresponds to a measurement to which the resistivity of the front metal grid does not contribute. The  $FF$ s measured with this sensing configuration and with negligible metal grid resistivity are thus identical. This sensing position represents the position of the average voltage distribution, so that the averages of voltage and current distributions are measured by the voltage and current contacts, respectively.

These explanations show that the choice of voltage sensing scheme significantly affects the measured solar cell performance. It is important to note that the strong influence of the sensing positions on the measured  $I$ - $V$  parameters is mainly caused by the fact that the resistivity of the fingers is orders of magnitude higher than the resistivity of the busbars.

### Influence of the number of current contacts

The differences in  $FF$  – and in efficiency  $\eta$  – between the sensing positions discussed above intensify with increasing grid resistivity (linearly by first approximation) and with increasing distance between the current contacts (quadratically by first approximation). Therefore, the impact of the sensing position is noticeably greater for a small number of current contacts and less pronounced for a larger number. This can be seen in Fig. 6, in which  $FF$  and  $\eta$  are shown as functions of the number of current contacts. For sensing at the current contact,  $FF$  and  $\eta$  increase with increasing numbers of contacts because the influence of the distributed series resistance decreases. For sensing in the middle, between the current contacts, the overestimation of  $FF$  and  $\eta$  is higher when there are fewer contacts, and decreases when the contact number increases. Sensing at the average potential in turn leads to  $FF$  and  $\eta$  measurements that are independent of the number of contacts. With this configuration, the grid-free  $I$ - $V$  parameters are always measured.

For large numbers of contacts, the three curves converge, as the voltage distribution in the fingers becomes so small that different sensing positions have negligible effects on the measurement. The convergence, however, is dependent on the grid resistivity: the spread of the curves increases considerably for higher grid resistivity, so that convergence occurs at larger numbers of contacts.

How does this impact the validity and assessment of measurement results of busbarless solar cells? Although the solar cell parameters used for the calculations are identical for all measurement configurations, the measured efficiencies can be very different and depend on the number of current contacts and the sensing design used. This explains why the different measurement systems from the previous section yield widely different results, and why the difference between them depends very much on the grid resistivity of the solar cells. For those solar cells, the effect is even twice as great, as it occurs on both the front and the rear side. Higher cell efficiencies therefore do not necessarily mean that the solar cells perform better – it could be that a different system was used for the measurement. For the sake of comparability, it is thus recommended to always specify the configurations used for the measurement of busbarless solar cells.

### Comparability with solar cells with busbars

Record solar cell efficiencies are essential yardsticks for highlighting outstanding achievements in solar cell research and industry. They can initiate new developments, but also decisions in opposition to apparently deficient concepts. It is therefore important to think about whether comparability exists for all solar cell concepts. In competition with conventional, busbar-based concepts, busbarless solar cell concepts in particular need to be critically assessed, given that the choice of measurement

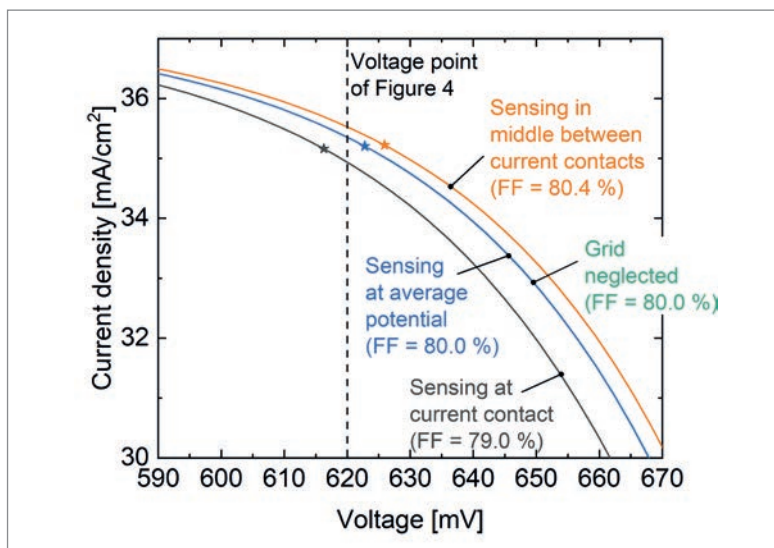


**Figure 5.** Calculated  $I$ - $V$  curves in the maximum power point region for different voltage sensing positions for the industrial SHJ solar cell (grid resistivity of  $50\text{m}\Omega/\text{cm}$ , nine current contacts). The dashed black line represents the voltage point for which the voltage and current density distributions in a grid finger are shown in Fig. 4. The voltage regions around short circuit and open circuit are not affected by the voltage sensing position. The stars indicate maximum power points.

**“The choice of voltage sensing scheme significantly affects the measured solar cell performance.”**

system has such a big impact on the measurement results of busbarless solar cells.

Further studies of the SHJ solar cells were therefore carried out. Front-grid resistivities in the range  $5\text{--}100\text{m}\Omega/\text{cm}$  were considered, and different busbar-based and busbarless configurations investigated: for the conventional solar cell concept with six busbars, a busbar shading of  $1.1\%_{\text{rel}}$  (corresponding to a busbar width of  $300\mu\text{m}$ ) and shading by the finger grid were taken into account. Current and voltage sensing was implemented at the busbars, in conformance with IEC standards (Fig. 7(a)). For the busbarless solar cell concepts, only the shading of the finger grid was accounted for (Fig. 7(b–e)). Various sensing configurations were considered, ranging from six current contacts (b) and (c), to 30 current contacts (d) and (e), additionally assuming different voltage sensing positions. Measurement configurations (a) and (b) in Fig. 7 allow a direct comparison to be made of busbar-based and busbarless solar cell concepts with similar contacting schemes. The number of current contacts is assumed to be identical, as is the voltage sensing – only the extent of shading differs. Both measurement configurations are oriented towards the interconnection of the solar cells in the module, and thus represent *realistic* contacting conditions.

As Fig. 7 shows, the measured efficiency is very much dependent on the grid resistivity for both measurement configurations. Because of the sensing at the current contact, the distributed series resistance of the metal grid contributes for both configurations. Higher efficiencies are measured for the busbarless concept: the difference in  $\eta$  amounts to as much as  $1.1\%_{\text{rel}}$  for all grid resistivities, which is exactly the same as the shading percentage of the busbars.

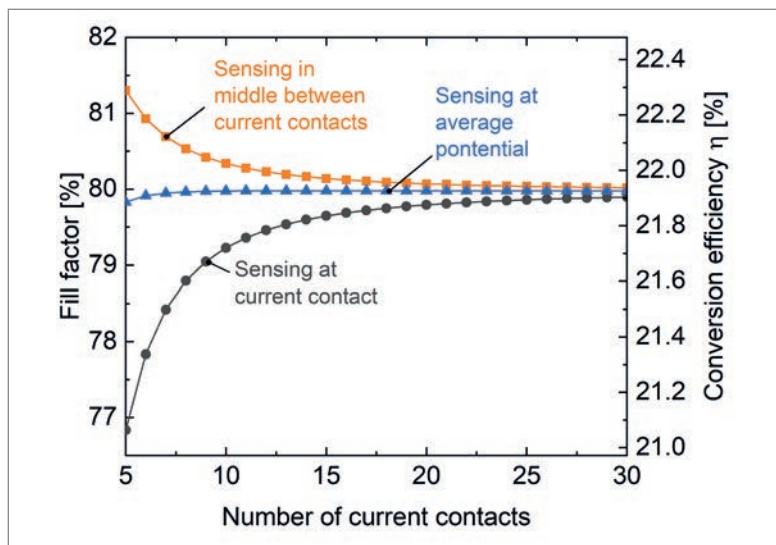


**Figure 6.** Calculated FF and  $\eta$  for an industrial SHJ solar cell (grid resistivity of  $50\text{m}\Omega/\text{cm}$ ), measured with a wire-based contacting unit, as a function of the number of current wires. The different colours represent the different voltage sensing positions discussed earlier. Note that for other grid resistivities, the influence of the sensing position can be smaller or larger.

For the other busbarless measurement configurations (c–e), the efficiency of the busbarless solar cells is measured to be higher. By either sensing the voltage at the average potential (c), or applying a large number of current contacts (d) and (e), the influence of the distributed series resistance of the finger grid is minimized. The measured efficiencies depend only slightly on grid resistivity. The measurement configurations (c–e) thus represent *idealized* contacting of busbarless solar cells, or scenarios where module integration is performed using an untypically large number of interconnectors. The difference in efficiency when compared with conventional, busbar-based solar cells (configuration (a)) is heavily dependent on grid resistivity: whereas the difference for low grid resistivity is only caused by busbar shading, the additional contribution of the distributed series resistance significantly increases with higher grid resistivity. Most of the difference is then caused by the series resistance of the front grid.

In conclusion, higher efficiencies are measured for busbarless solar cell concepts than for conventional, busbar-based concepts – how much higher depends not only on busbar shading and grid resistivity, but also on the contacting scheme used for the measurement. Manufacturers and researchers therefore need to be aware of how to assess and compare the efficiency values reported for busbarless solar cells with each other, and especially with the efficiency values of conventional solar cells.

Measuring a high efficiency at the solar cell level does not automatically mean that the solar module assembled from these cells will also have a similar high efficiency. If the cell efficiency is overrated with

**“Higher cell efficiencies do not necessarily mean that the solar cells perform better – it could be that a different system was used for the measurement.”**

regard to module application, the CTM loss will be considerably affected. This issue will be discussed in more detail in the following section.

### Implications for CTM losses

In order to estimate the power of a solar module assembled using the industrial SHJ solar cells, the sophisticated calculation software SmartCalc.CTM [11,23] is applied. This software uses  $I$ – $V$  parameters and spectrally dependent reflectance and quantum efficiencies of the solar cells, as well as geometric specifications of the cells, interconnectors and solar module stack as input data. A virtual twin of the solar module is created which can be analysed with respect to optical, electrical, thermal and geometrical loss channels.

### Model for calculating CTM losses

The solar cell specifications used for the CTM calculations are based on the same industrial SHJ solar cells examined in the previous sections. Spectral reflectance and quantum efficiencies are taken from measurements, and the  $I$ – $V$  parameters are determined using the independent diode model. Different front-grid resistivities, ranging from 5 to  $100\text{m}\Omega/\text{cm}$ , were again considered, as well as the different sensing configurations in Fig. 7. For the conventional solar concept with six busbars, busbar widths of  $300\mu\text{m}$  were again assumed. For larger numbers of busbars, a realistic grid layout consisting of 20 pads per busbar and a supporting grid line with a width of  $100\mu\text{m}$  in between was employed. In order to be sensitive to the effects of front contacting only, all solar cells were considered to be monofacial.

For solar cell interconnection, advanced interconnector specifications were used: for the conventional solar cell concept with six busbars, rectangular, coated copper ribbons with a width of  $0.6\text{mm}$  and a height of  $0.25\text{mm}$  were utilized. For the busbarless solar cell concept with six interconnectors, six wires with a diameter of  $0.4\text{mm}$  were assumed. In the case of solar cells with a larger number of interconnectors, wires with a slightly reduced diameter of  $0.35\text{mm}$  were employed.

Typical module specifications were used: the module contains 60 solar cells, a polyolefin encapsulant, an aluminium backsheet and low-iron glass with an anti-reflective coating and a thickness of  $3.2\text{mm}$ . The module dimensions are  $1.70 \times 1.00\text{m}^2$ .

With the use of these data, the optical and electrical gains and losses are calculated and the module power predicted. The CTM power ratio is calculated by comparing the module power with the summed power of the solar cells. CTM values greater than 100% represent a power gain of the solar cells as a result of module assembly with respect to the cell measurement, while values less than 100% represent a power loss.

### CTM losses for six interconnectors

Fig. 8 shows the calculated CTM power ratios for the industrial SHJ solar cells with six interconnectors

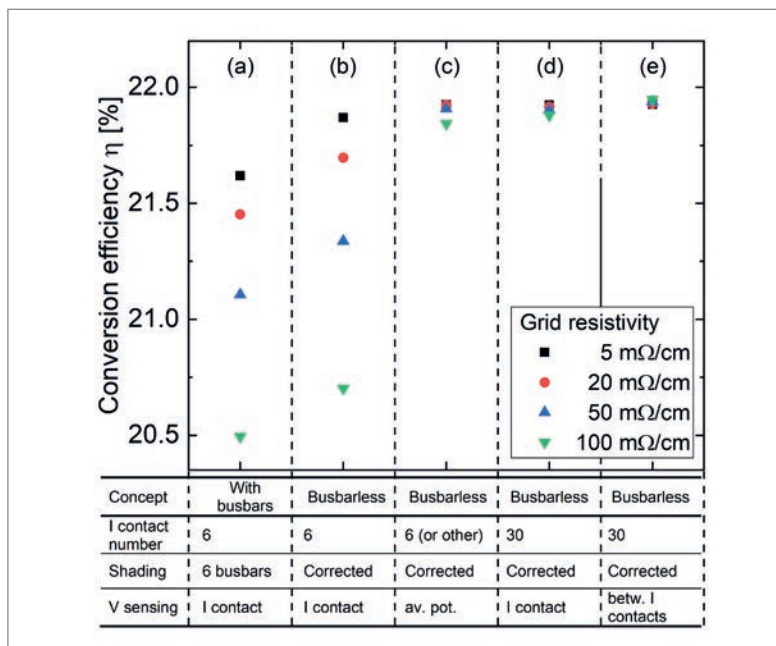


**Figure 7. Calculated conversion efficiencies  $\eta$  for industrial SHJ solar cells with front-grid resistivities in the range 5–100m $\Omega$ /cm. Different measurement configurations were assumed, representing the same solar cell with (a) six busbars or (b–e) without busbars. For the busbarless configurations, different numbers of current contacts and voltage sensing positions were considered.**

and the busbar concepts and measurement configurations detailed in the previous section.

Solar modules assembled from solar cells of a certain grid resistivity yield practically the same power, no matter what the value of efficiency measured by the cell measurement. Only small differences between busbar-based and busbarless concepts result from slightly different optical and resistive losses. The solar module power is therefore nearly independent of the cell measurement configurations, and only depends on the grid resistivity: the module power decreases almost linearly with increasing grid resistivity as a result of the increasing distributed series resistance of the grid. Because the measured cell power is highly dependent on the cell measurement configurations (which are affected by the grid resistivity in different ways), the CTM ratios are significantly affected by the cell measurement configurations as well.

Configuration (a) in Fig. 8 represents a conventional solar cell concept with six busbars, configurations (b–e) busbarless solar cell concepts with different numbers of current contact and different voltage sensing position. It can be seen that all solar cell concepts suffer a loss in power as a result of module assembly, chiefly caused by optical losses – such as shading of the active solar cell area by the interconnectors, and front glass reflection – but also by ohmic losses within the interconnectors. The exact extent of the CTM loss depends very much on

**“Measuring a high efficiency at the solar cell level does not automatically mean that the solar module assembled from these cells will also have a similar high efficiency.”**

the specific measurement concept, the grid resistivity and interconnector design.

The conventional, busbar-based solar cell concept has CTM ratios closest to unity of all configurations. For this configuration, the measured solar cell power gives a significant and reliable prediction of the later module power. The CTM ratios are particularly not dependent on the grid resistivity, as the resistive losses of the front grid of the solar cells in the module are correctly considered by the cell measurement. Since the busbar already shades active solar cell area, additional shading from the rectangular interconnector ribbons protruding from the busbars is limited in module integration: parts of the shading loss are already incorporated in the cell measurement. Therefore, a higher CTM ratio is achieved.

The module power decreases with increasing grid resistivity because of the increasing distributed series resistance of the grid. Solar cell measurements with more *realistic* sensing conditions (b) consider this increasing resistive loss, so that the CTM ratio is virtually independent of the grid resistivity. Since the number of wires is the same in cell characterization and module integration, the grid losses are already incorporated in the cell characterization. Solar cell measurement and module output show the same decrease in power with increasing grid resistivity. As the cross sections of the interconnecting wires are smaller than the cross sections of the rectangular ribbons, the CTM ratios are further reduced because of resistive losses. Additionally, shading of active solar cell area, which is not taken into account in the cell measurement, leads to reduced CTM ratios. However, as the optically relevant diameter of the wires is only 60% of the total diameter because of reflection to the solar cell surface [24], this decrease is small. Realistic cell measurement configurations can therefore predict module performance fairly reliably.

Solar cell measurements with *idealized* sensing have yielded efficiencies that are almost independent of grid resistivity, because the influence of the distributed series resistance of the grid has been minimized by adapted contacting or voltage sensing. This now has a significant effect on the CTM ratios for these measurement configurations (c–e). For low grid resistivity, the resistive grid losses are small and only wire shading prevails. The CTM ratios are thus close to the measurements obtained with realistic sensing configurations. For high grid resistivity, however, the contribution of the distributed series resistance increases more and more. The CTM ratios thus decrease almost linearly to fairly low values with increasing grid resistivity. Idealized cell measurement configurations therefore provide a rather poor and unreliable estimate of the performance of the cells in a module.

#### **CTM losses for a larger number of interconnectors**

For higher grid resistivity, it is often beneficial in terms of module performance to increase the number of interconnectors. An additional analysis was

therefore performed to assess the influence of the number of interconnectors on the CTM ratio. Fig. 9 shows the corresponding results for both realistic and idealized measurement of busbarless solar cells.

In the case of the realistic measurement configuration (b), the CTM ratios are virtually independent of the number of interconnectors and the grid resistivity, since cell measurements and module output power are similarly affected by resistive grid losses. For larger numbers of interconnectors, the loss caused by shading of interconnectors in the module, which increases quadratically with the shading fraction, becomes significant and the CTM is slightly reduced. The realistic cell measurement configuration reliably predicts module performance for various numbers of interconnectors and grid resistivities.

The CTM ratio for the idealized measurement configuration (e) is affected by two contrasting contributions: on the one hand, the resistive grid losses (which are not detected by cell measurement) decrease for increasing number of interconnectors, while, on the other hand, the shading losses increase. For low grid resistivity, shading losses prevail and the CTM ratios decrease with increasing number of interconnectors. For high grid resistivity, however, resistive losses are dominant and the CTM ratios are higher when more interconnectors are used. Although the quality with which the module performance is predicted by this idealized measurement configuration improves for a larger number of interconnectors, it is highly dependent on the number of interconnectors and on grid resistivity. Module power output is therefore only predicted to a limited extent by idealized cell measurements.

### The best way to measure busbarless solar cells

The range of possibilities for measuring busbarless solar cells raise the question as to what the most meaningful way of measuring these solar cells actually is. Two main approaches have become apparent from the above discussions: measuring busbarless solar cells according to (1) realistic or (2) idealized module application.

#### (1) Measurements according to realistic module application

Measurements according to realistic module application means that the number of current contacts should be chosen identical to that of the later module application; for example, solar cells intended for interconnection with, say, 12 wires should also be measured using 12 current contacts. Voltage sensing should be carried out at the current contact in order to fully consider the distributed series resistance of the grid. Shading by the contact units should be corrected: although the obvious differences between busbar-based and busbarless concepts fuel the discussion about whether shading by contact bars or wires should be taken into account, in the authors' opinion the comparability

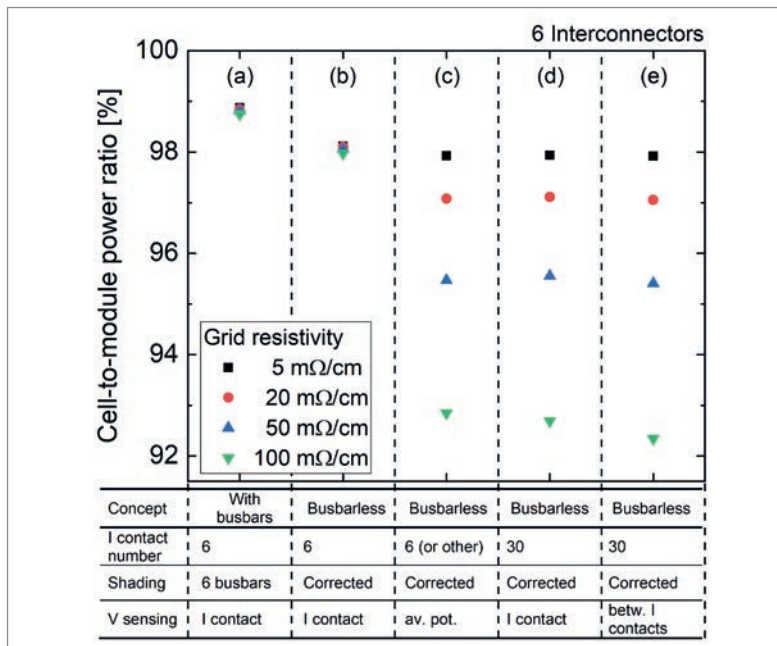


Figure 8. Calculated CTM power ratios for industrial SHJ solar cells with front-grid resistivities ranging from 5 to 100mΩ/cm, assembled in modules with six interconnectors. The configurations in Fig. 7 were used for contacting and voltage sensing.

**“Realistic cell measurement configurations can predict module performance fairly reliably, whereas idealized configurations provide a rather poor and unreliable estimate.”**

of measurement results between different solar simulators needs to be ensured (dependence on the divergence). This can best be realized by correcting for shading. Moreover, and most importantly, the majority of measurement systems bear no resemblance whatsoever with interconnectors in the module and cast a very different shadow.

The *I-V* parameters of busbarless solar cells measured this way provide the best approximation of the values that can be expected in the module, because the CTM losses are minimized. However, the exact same cell can exhibit very different efficiencies depending on how the cell is integrated in the module. Moreover, how the cell will be interconnected in the module must already be known before the measurement of the cell takes place, which is not always the case. This approach furthermore poses tremendous requirements on measurement equipment, as various module layouts may need to be contemplated.

Implementing this measurement approach is rather complicated. To the authors' knowledge, there is currently no system commercially available on the market with current and voltage contacts located directly on the solar cell grid which are electrically isolated but close to each other. The complexity lies in the high finger resistivity, which requires either very low distances of the order of 100µm or less between adjacent current and voltage contacts, or the realization of isolated current-voltage-current contact triplets [19].

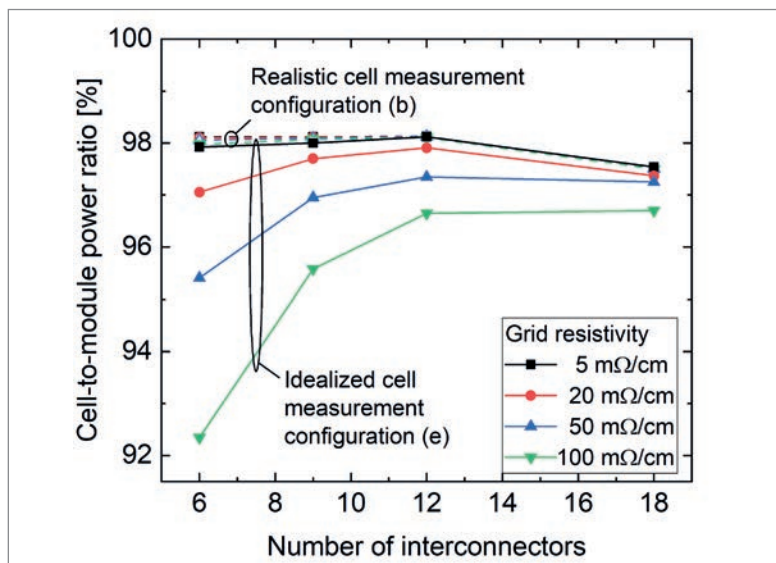


**Figure 9.** Calculated CTM ratios as a function of the number of interconnectors, for busbarless SHJ solar cells measured with a realistic configuration (b) (open symbols) and with an idealized configuration (e) (closed symbols). Different front-grid resistivities ranging from 5 to 100 mΩ/cm were considered. In configuration (b), the number of current contacts for the measurement was assumed to be equal to the number of interconnectors in the module.

## (2) Measurements according to idealized module application

In idealized conditions, busbarless solar cells should be measured either with a large number of current contacts or with voltage sensing at the average potential. This way, the front-grid resistivity does not contribute to the measurement. Shading by the contact unit needs to be corrected. This measurement configuration thus resembles an idealized module interconnection with a large number of shadow-free contacts.

There are several systems available on the market that are well-suited to idealized measurements. This measurement approach has the advantage that only one cell efficiency is measured which is independent of module application and quantifies the potential of the solar cell. However, the measured  $I$ - $V$  parameters are the same for solar cells with different front-grid resistivities, as this resistivity is not taken into account. This poses the danger of solar cell development decoupled from module applications – at least for non-vertically integrated manufacturers. An increase in solar cell efficiency could be accompanied by a similar increase in CTM losses and a stagnation, or even a decrease, in module efficiency. Moreover, in the race for the best solar cell efficiencies, the competition between busbar-based and busbarless solar cells is rather unbalanced, as the efficiencies of busbarless solar cells are clearly inflated. In extreme cases, for record cell devices, the finger widths of busbarless cells could be designed much smaller than necessary in the module, as the resistance is not relevant.

**“For both realistic and idealized approaches it is highly recommended to report not only which efficiency value has been measured for a busbarless solar cell, but also *how* it has been measured.”**

The comparatively high efficiencies of busbarless solar cells also need to be regarded as critical in terms of costs: non-vertically integrated module manufacturers, who purchase solar cells from a cell producer for module assembly, need to be aware that they may pay an inflated price for the solar cells. The revenue for the modules might be significantly lower because of the high CTM losses – the idealized cell measurement has concealed relevant resistive grid losses. Module manufacturers need to be aware of the measurement conditions leading to the power labelling of their solar cell purchase. A solution to this issue could be transparency of the measurement conditions and a subsequent consideration of shading and resistive losses by the calculations.

It is evident that there are advantages and disadvantages associated with the two measurement approaches, both in terms of the significance and the comparability of the measurement results, and in terms of system availability. For both realistic and idealized approaches, it is highly recommended to report not only which efficiency value has been measured for a busbarless solar cell, but also *how* it has been measured. This facilitates the assessment and interpretation of the measurement results. In any case, manufacturers and investors should be well aware that there can be hidden losses associated with busbarless solar cells.

## Acknowledgements

The work reported in this paper was partly supported by the German Federal Ministry for Economic Affairs and Energy within the framework of the BiZePS-PLUS project (Contract No. 03EE1064). The authors would like to thank K. Bothe and D. Hinken for fruitful discussions.

## References

- [1] Lorenz, A., Linse, M., Frintrup, H. et al. 2018, “Screen-printed thick film metallization of silicon solar cells – Recent developments and future perspectives”, *Proc. 35th EU PVSEC*, Brussels, Belgium, p. 819.
- [2] VDMA 2020, “International technology roadmap for photovoltaic (ITRPV): Results 2019”, 11th edn (Apr.) [<https://itrpv.vdma.org/en/>].
- [3] Walter, J., Tranitz, M., Volk, M. et al. 2014, “Multi-wire interconnection of busbar-free solar cells”, *Energy Procedia*, Vol. 55, p. 380.
- [4] Geipel, T., Huq, M. & Eitner, U. 2014, “Reliable interconnection of the front side grid fingers using silver reduced conductive adhesives”, *Energy Procedia*, Vol. 55, p. 336.
- [5] Söderström, T., Papet, P. & Ufheil, J. 2013, “Smart Wire Connection Technology”, *Proc. 28th EU PVSEC*, Paris, France, p. 495.
- [6] IEC 60904-1: 2006, “Photovoltaic devices – Part 1: Measurement of photovoltaic current-voltage characteristics”, 2nd edn.
- [7] Hohl-Ebinger, J., Grote, D., Hund, B. et al. 2008,

“Contacting bare solar cells for STC measurements”, *Proc. 23rd EU PVSEC*, Valencia, Spain, p. 2012.

[8] Kruse, C., Wolf, M., Schinke, C. et al. 2017, “Impact of contacting geometries when measuring fill factors of solar cell current–voltage characteristics”, *IEEE J. Photovolt.*, Vol. 7, No. 3, p. 747.

[9] Bothe, K. & Hinken, D. 2019, “Precise and accurate solar cell measurements at ISFH CalTeC”, *Photovoltaics International*, 43rd edn, p. 44.

[10] Hädrich, I., Eitner, U., Wiese, M. et al. 2014, “Unified methodology for determining CTM ratios: Systematic prediction of module power”, *Sol. Energy Mater. Sol. Cells*, Vol. 131, p. 14.

[11] Mittag, M. & Ebert, M. 2017, “Systematic PV module optimization with the cell-to-module (CTM) analysis software”, *Photovoltaics International*, 36th edn, p. 97.

[12] Bassi, N., Clerc, C., Pelet, Y. et al. 2014, “GridTOUCH: Innovative solution for accurate IV measurement of busbarless cells in production and laboratory environments”, *Proc. 29th EU PVSEC*, Amsterdam, The Netherlands, p. 1180.

[13] Ramspeck, K., Waleska, P., Schenk, S. et al. 2019, “Contacting new solar cell metallization layouts and contact quality surveillance in solar cell production”, *Proc. 36th EU PVSEC*, Marseille, France, p. 443.

[14] Kamatani, K., Fujita, Y., Takeda, Y. et al. 2019, “Development of new probe bar for c-Si PV cells with unique electrode design such as busbar-less, multi busbar and complicated busbar”, *Proc. 36th EU PVSEC*, Marseille, France, p. 384.

[15] Bothe, K. 2019, “Contacting busbarless (BBo) solar cells at ISFH CalTeC, Technical information” (description of pv-tools) [[https://isfh.de/wp-content/uploads/2019/12/ISFH-CalTeC\\_BBoContacting\\_19b.pdf](https://isfh.de/wp-content/uploads/2019/12/ISFH-CalTeC_BBoContacting_19b.pdf)].

[16] INGUN Pruefmittelbau, Personal communication.

[17] Braun, S. 2014, “Simulation, Analyse und Herstellung von kristallinen Si-Solarzellen mit Multi-Busbar-Verschaltung”, Dissertation, University of Konstanz, Germany, p. 108.

[18] Raj, S., Wong, J., Ramprasad, S. et al. 2018, “Effective I-V measurement techniques for busbarless and multi-busbar solar cells”, *Proc. 7th WCPEC*, Waikoloa, Hawaii, USA, p. 3294.

[19] Rauer, M., Kordelos, K., Krieg, A. et al. 2019, “Accurate measurement of busbarless silicon solar cells”, *Proc. 8th Worksh. Metalliz. Interconn. Cryst. Sil. Sol. Cells*, Konstanz, Germany.

[20] Geisemeyer, I., Kallies, C., Hohl-Ebinger, J. et al. 2014, “Contacting bare silicon solar cells with advanced cell metallisation”, *Proc. 29th EU PVSEC*, Amsterdam, The Netherlands, p. 1202.

[21] Fischer, B., Fath, P. & Bucher, E. 2000, “Evaluation of solar cell J(V)-measurements with a distributed series resistance model”, *Proc. 16th EU PVSEC*, Glasgow, UK, p. 1365.

[22] Greulich, J., Glatthaar, M., Krieg, A. et al. 2009, “JV characteristics of industrial silicon solar cells: Influence of distributed series resistance and Shockley Read Hall recombination”, *Proc. 24th EU PVSEC*, Hamburg, Germany, p. 2065.

[23] Fraunhofer ISE 2020, “SmartCalc.CTM” [[www.cell-to-module.com](http://www.cell-to-module.com)].

[24] Mittag, M., Beinert, A.J., Rendler, L. et al. 2016, “Triangular ribbons for improved module efficiency”, *Proc. 32nd EU PVSEC*, Munich, Germany, p. 169.

**About the Authors**



Michael Rauer received his Ph.D. from the University of Konstanz, Germany, in 2014, in collaboration with Fraunhofer ISE. In 2015 he was awarded the SolarWorld Junior Einstein Award for his research on aluminium-alloyed contacts. He is currently working at CalLab PV Cells on the measurement of novel silicon solar cells.



Alexander Krieg studied renewable energy systems at the University of Applied Sciences Berlin and received his master’s in 2007. He is currently working as a scientist in the inline solar cell analytics and simulation group at Fraunhofer ISE.



Andrea Pfreundt holds degrees in physics and nanoscience. She obtained her Ph.D. in 2015 from the Technical University of Denmark, for research on nanowire biomedical devices. In 2017 she joined Fraunhofer ISE in the module technology department, where her focus is on model development for module efficiency analysis.



Max Mittag is the head of the PV module simulation team at Fraunhofer ISE. His current work includes analysis of power losses in PV modules (cell-to-system analysis), and techno-economical assessments as well as multi-physics simulation and development of new PV module concepts.



Sebastian Pingel received his Diploma in physics in 2006 from the University of Hamburg, in collaboration with Fraunhofer ISE. He held various positions at Solon R&D, First Solar and PI-Berlin, before joining Helmholtz Center Berlin (HZB), where he started working in the field of SHJ cells. Since 2018 he has been employed as a scientist at Fraunhofer ISE.

**Enquiries**

Michael Rauer  
 Fraunhofer Institute for Solar Energy Systems ISE  
 Heidenhofstraße 2, 79110 Freiburg, Germany

Tel: +49(0)761/4588-5564  
 Email: michael.rauer@ise.fraunhofer.de